NeuroImage 63 (2012) 1257–1272

Contents lists available at SciVerse ScienceDirect

NeuroImage

journal homepage: www.elsevier.com/locate/ynimg

Larger is twistier: Spectral analysis of gyrification (SPANGY) applied to adult brain size polymorphism

David Germanaud [a,b,i,*,1], Julien Lefèvre [c,d,**,1], Roberto Toro [e,f], Clara Fischer [g], Jessica Dubois [h,i], Lucie Hertz-Pannier [a,b,i], Jean-Francois Mangin [g,i]

[a] UMR663, INSERM-Université Paris Descartes, Paris, France
[b] CEA, I2BM, DSV, NeuroSpin, LBIOM, Gif/Yvette, France
[c] Aix-Marseille Université, Département d'Informatique, Marseille, France
[d] CNRS, LSIS, UMR 7296, Marseille, France
[e] Human Genetics and Cognitive Functions, Institut Pasteur, Paris, France
[f] CNRS URA 2182, Genes, synapses and cognition, Institut Pasteur, Paris, France
[g] CEA, DSV, I2BM, Neurospin, LNAO, France
[h] U992, INSERM, NeuroSpin, Gif/Yvette, France
[i] IFR49, NeuroSpin, Gif/Yvette, France

ARTICLE INFO

Article history:
Accepted 23 July 2012
Available online 2 August 2012

Keywords:
Gyrification
MRI
Spectral analysis
Laplace–Beltrami operator
Computational anatomy
Segmentation
Allometry

ABSTRACT

The description of cortical folding pattern (CFP) is challenging because of geometric complexity and inter-subject variability. On a cortical surface mesh, curvature estimation provides a good scalar proxy of CFP. The oscillations of this function can be studied using a Fourier-like analysis to produce a power spectrum representative of the spatial frequency composition of CFP. First, we introduce an original method for the SPectral ANalysis of GYrication (Spangy), which performs a spectral decomposition of the mean curvature of the grey/white interface mesh based on the Laplace–Beltrami operator eigenfunctions. Spangy produces an ordered 7 bands power spectrum of curvature (B0–B6) and provides an anatomically relevant segmentation of CFP based on local spectral composition. A spatial frequency being associated with each eigenfunction, the bandwidth design assumes frequency doubling between consecutive spectral bands. Next, we observed that the last 3 spectral bands (B4, 5 and 6) accounted for 93% of the analyzed spectral power and were associated with fold-related variations of curvature, whereas the lower frequency bands were related to global brain shape. The spectral segmentation of CFP revealed 1st, 2nd and 3rd order elements associated with B4, B5 and B6 respectively. These elements could be related to developmentally-defined primary, secondary and tertiary folds. Finally, we used allometric scaling of frequency bands power and segmentation to analyze the relationship between the spectral composition of CFP and brain size in a large adult dataset. Total folding power followed a positive allometric scaling which did not divide up proportionally between the bands: B4 contribution was constant, B5 increased like total folding power and B6 much faster. Besides, apparition of new elements of pattern with increasing size only concerned the 3rd order. Hence, we demonstrate that large brains are twistier than smaller ones because of an increased number of high spatial frequency folds, ramifications and kinks that accommodate the allometric increase of cortical surface.

Introduction

The description of human cortical folding remains a major challenge for neuroimaging due to its great complexity and variability. Beyond an interest in gyrification itself, a better knowledge of cortical folding would allow us to device more precise methods for inter-individual comparisons as research reveals subtle correlations with typical and pathological functioning (Fischl et al., 2007; Cachia et al., 2008). Sulci have been traditionally classified from a developmental point of view into primary, secondary and tertiary (Chi et al., 1977) according to their order of appearance during fetal life and early childhood. But cortical folding is probably a more continuous process than that suggested

* Correspondence to: D. Germanaud, UMR663, INSERM-Université Paris Descartes, Paris, France.
** Correspondence to: J. Lefèvre, Aix-Marseille Univ, Département d'Informatique, Marseille, France.
E-mail addresses: david197@free.fr (D. Germanaud), julien.lefevre@univ-amu.fr (J. Lefèvre), rto@pasteur.fr (R. Toro), clara.fischer@cea.fr (C. Fischer), jessica.dubois@cea.fr (J. Dubois), lucie.hertz-pannier@cea.fr (L. Hertz-Pannier), jean-francois.mangin@cea.fr (J.-F. Mangin).
[1] These authors contributed equally to this work.

1053-8119/$ – see front matter © 2012 Elsevier Inc. All rights reserved.
http://dx.doi.org/10.1016/j.neuroimage.2012.07.053

by this classification (Armstrong et al., 1995), and morphological features resulting from successive folding phases likely intricate into the same given fold (Paus et al., 1996). This interaction between folding phases leads to a geometric complexity well described for the central sulcus (White et al., 1997): sulci are not straight objects but show ramifications, digitations, nodes, dimples, etc. This complexity is associated with an important inter-individual variability (Yousry et al., 1997; Régis et al., 2005) which complicates the construction of folding atlases, even at a large-scale level. Eventually, as soon as mature gyrification is achieved, it is very difficult to attribute, based on morphological features alone, a primary, secondary or tertiary character to a given piece of a cortical fold.

In the general population, human brain size is also highly variable, with the largest adult brains having up to 2 times the volume of the smallest ones (Milner, 1990; Whitwell et al., 2001). As for many biological objects, the relationship between cortical surface geometry (shape) and brain volume (size) is not simply homothetic: there are shape modifications coming with size variations (allometry). Across mammals, cortical surface area appears to scale proportionally with brain volume, i.e. with a scaling exponent around 1, whereas an isometric relationship would predict a scaling exponent of 2/3 (Prothero and Sundsten, 1984) (Fig. 1c). A similar allometric scaling can be observed among humans, with scaling exponents in the order of 0.8 to 0.9 (Im et al., 2008; Toro et al., 2008). Indeed, large brains show a relative excess of cortical surface, which is accommodated by an increase in folding. Several gyrification indexes have been proposed at hemispheric (Zilles et al., 1988) or local levels (Schaer et al., 2008; Toro et al., 2008). They measure the proportion of cortical surface buried by folding, but are unable to distinguish between an increase in fold depth and an increase in fold number or ramification. Such a modification of the complexity of cortical folding pattern (CFP) with brain size is nonetheless suspected: larger brains seem twistier (Fig. 1a). So far, there have been a few attempts to propose a more descriptive quantitative assessment of gyrification complexity but there is still no consensual measure, even at the hemispheric level (Luders et al., 2004; Yotter et al., 2011). From a theoretical perspective, several models suggest that folding in an expanding domain should lead to the development of branching with doubling of the spatial frequency patterns (Fig. 1b). This phenomenon is observed with reaction–diffusion (Crampin et al., 1999; Striegel and Hurdal, 2009) and mechanical models (Mora and Boudaoud, 2006), but also with fractal approaches (Thompson et al., 1996; Yotter et al., 2011). Thus, the study of the spatial frequencies of CFP should provide us with an interesting new measure of gyrification complexity.

The folded surface of a brain hemisphere can be viewed as a closed surface of zero-genus (Dale et al., 1999) on which it is possible to map scalar functions estimating surface characteristics such as curvature or sulcal depth. Theses oscillatory functions can be taken as proxies of the hemispheric gyrification that allow the study of CFP properties through the analysis of its spatial oscillation frequencies. This spectral approach can be used to produce a power spectrum representative of the spatial frequencies composition of a folded surface. Such a generalization of Fourier analysis is performed with the eigenfunctions of the Laplace–Beltrami Operator (LBO), which provides a natural approach to obtain spectral decompositions on surfaces or, more generally, Riemannian manifolds (Berger, 2003). The methods to apply this mathematical theory to the analysis of discrete meshes have been recently described by Reuter et al. (2006) and Lévy (2006). Compared with the more traditional spherical harmonics decomposition (Chung et al., 2008; Hübsch and Tittgemeyer, 2008), this approach has the advantage of a direct processing of native data without nonlinear alignment and spherical parameterization steps. Indeed, such a parameterization induces a certain level of both distance or angular distortions (Gu et al., 2004; Kruggel, 2008) since folding wavelengths in the native surface are basically projected onto the sphere with a different wavelength. Recently it has also revealed a better information compaction than spherical harmonics (Seo and Chung, 2011). In return, LBO-based spectral analysis requires to device an appropriate strategy to compare individually defined decompositions (Knossow et al., 2009).

In this article, we propose an original method for the Spectral Analysis of Gyrification (Spangy) which produces a morphologically relevant band power spectrum of CFP. We also report on the interest of Spangy for the study of the relationship between CFP complexity and brain size in the large cohort of young healthy adults of the ICBM MRI database (Mazziotta et al., 1995; Watkins et al., 2001). Firstly, we present theoretical and numerical aspects of the LBO-based spectral analysis, along with relevant Spangy design choices such as definition of curvature function, spatial frequencies, spectral bands or spectral segmentation of CFP. Next, we derive the measuring and describing properties of Spangy from our numerical and anatomical results in the ICBM database. Finally, we establish the relationship between spectral composition of CFP and brain size through allometric scaling. To our knowledge, this is the first time that a LBO-based spectral analysis is used to provide a relevant signature of CFP and assess gyrification complexity.

Materials and methods

Data set

Subjects

We analyzed the 152 normal volunteers of the ICBM MRI database (Watkins et al., 2001). Each subject had a T1-weighted scan (3D fast field echo images, 140 to 160 slices, 1 mm isotropic resolution, TR = 18 ms, TE = 10 ms, flip angle = 30, Phillips Gyroscan 1.5 T scanner). One scan was excluded because of poor quality, leading to artifacts in the automatic segmentation step. Of the remaining 151 subjects, 86 were males and 65 were females. Ages ranged from 18 to 44 years (mean age: 25 years, standard deviation: 4.9 years). 128 subjects were right-handed, 14 were left-handed, and handedness was unknown for the remaining 10.

Brain segmentation and morphometric parameters

T1-weighted images were automatically segmented with BrainVISA T1 segmentation pipeline (BrainVisa Software) to obtain topologically spherical mesh reconstructions of the left hemispheric hull (morphological closing of the hemispheric mask) and grey-white interface. The reconstructions were visually inspected for segmental disruption or excess of surface spicules, leading to the exclusion of one subject. The hemispheric volume (HV), i.e. the volume inside the hemispheric hull and the hemispheric surface area (HA), i.e. the area of the grey-white interface, were computed for each left hemisphere using the BrainVISA Morphometry toolbox. We used the mean curvature (C) of the grey-white interface to represent CFP. It was computed with the non-parametric estimator implemented in the BrainVISA Surface toolbox, which is based on the method introduced by Desbrun et al. (1999).

Spectral analysis of curvature

See Fig. 2 for steps summary.

Laplace–Beltrami operator and spectral theory: eigenfunction basis computation (step 1)

Given a compact Riemannian manifold $(\mathcal{M}, g)$, where g is a metric tensor, we introduce $L^2(\mathcal{M}) = \left\{u\colon \mathcal{M} \to \mathbb{R} / \int_{\mathcal{M}} u^2 < +\infty\right\}$ and the scalar product $<u, v> = \int_{\mathcal{M}} uv$. The spectrum of the *Laplace–Beltrami operator* (LBO) $\Delta_{\mathcal{M}} = \mathrm{div} \circ \nabla_{\mathcal{M}}$ is discrete (Berger, 2003). We denote $\lambda_0 = 0 \leq$

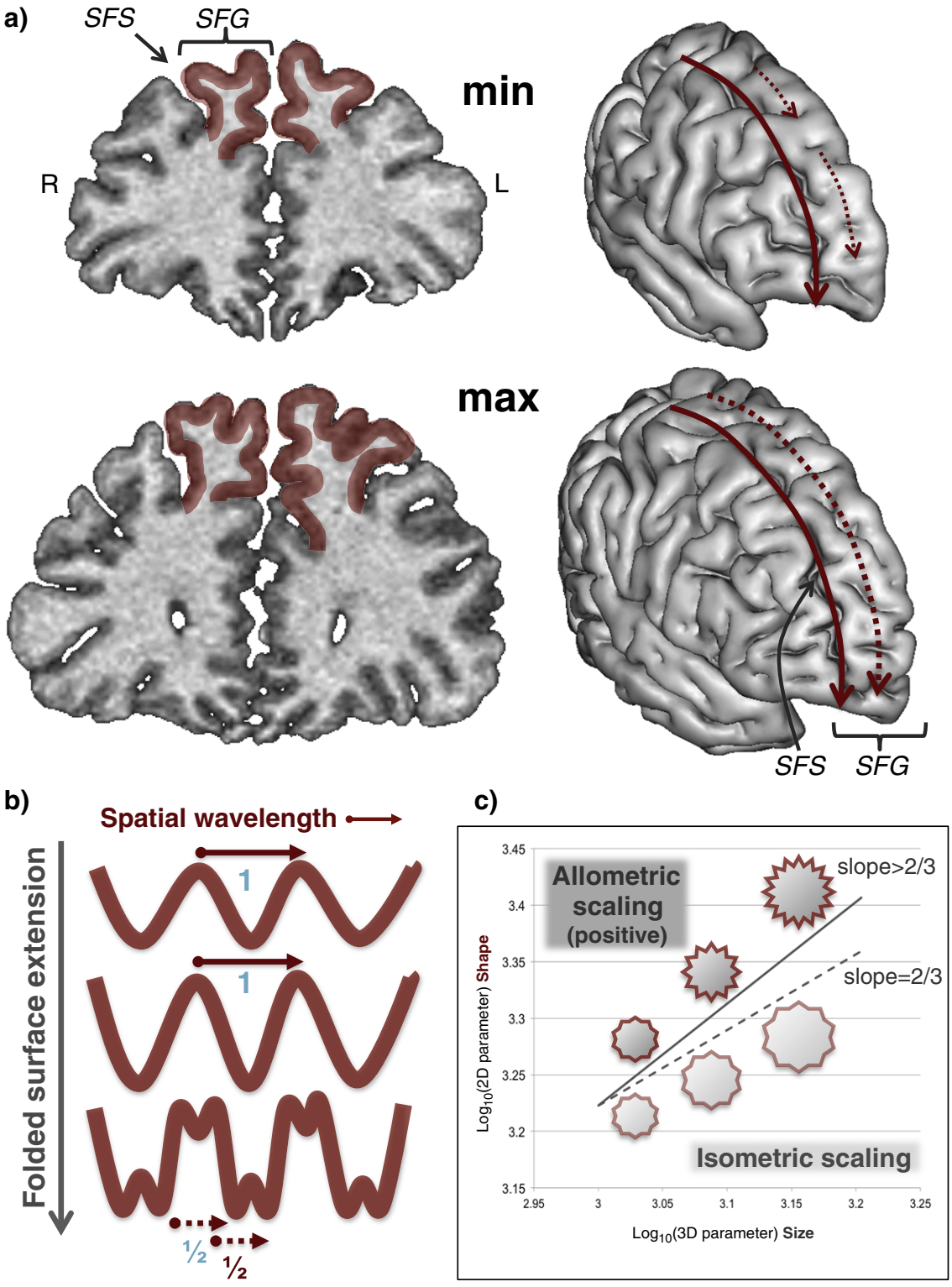

Fig. 1. Modeling framework for cortical folding. a) Larger seems twistier Left: coronal section perpendicular to the ACPC line and tangential to the genu of the corpus callosum (T1-weighted images). Right: pial surface of the right hemisphere (Morphologist, BrainVISA). 1st row: smallest brain of the database. 2nd row: largest brain of the database. The large brain shows a more folded cortical surface in the SFG and a more complex pattern of the SFS with an almost doubling in relative spatial frequency of the folds. SFS: superior frontal sulcus, SFG: superior frontal gyrus, R: right, L: left. b) The doubling frequency hypothesis Theoretical model of folded surface extension extrapolated from Mora and Boudaoud (2006): first the folded surface extension leads to an increase in the depth of the folds, secondly it comes to a point when new folds appear with twice the initial spatial frequency. c) Allometric scaling for cortical surface geometry. Isometric scaling occurs when there is an homothetic transformation between small and large brains. The exponent of the power scaling law between 2-dimensional (surface, shape) and 3-dimensional (size) parameters is 2/3. The shape is constant. Allometric scaling occurs when shape modification, such as an increase in cortical folding pattern complexity, comes with size variation. The exponent of the power scaling law is >2/3.

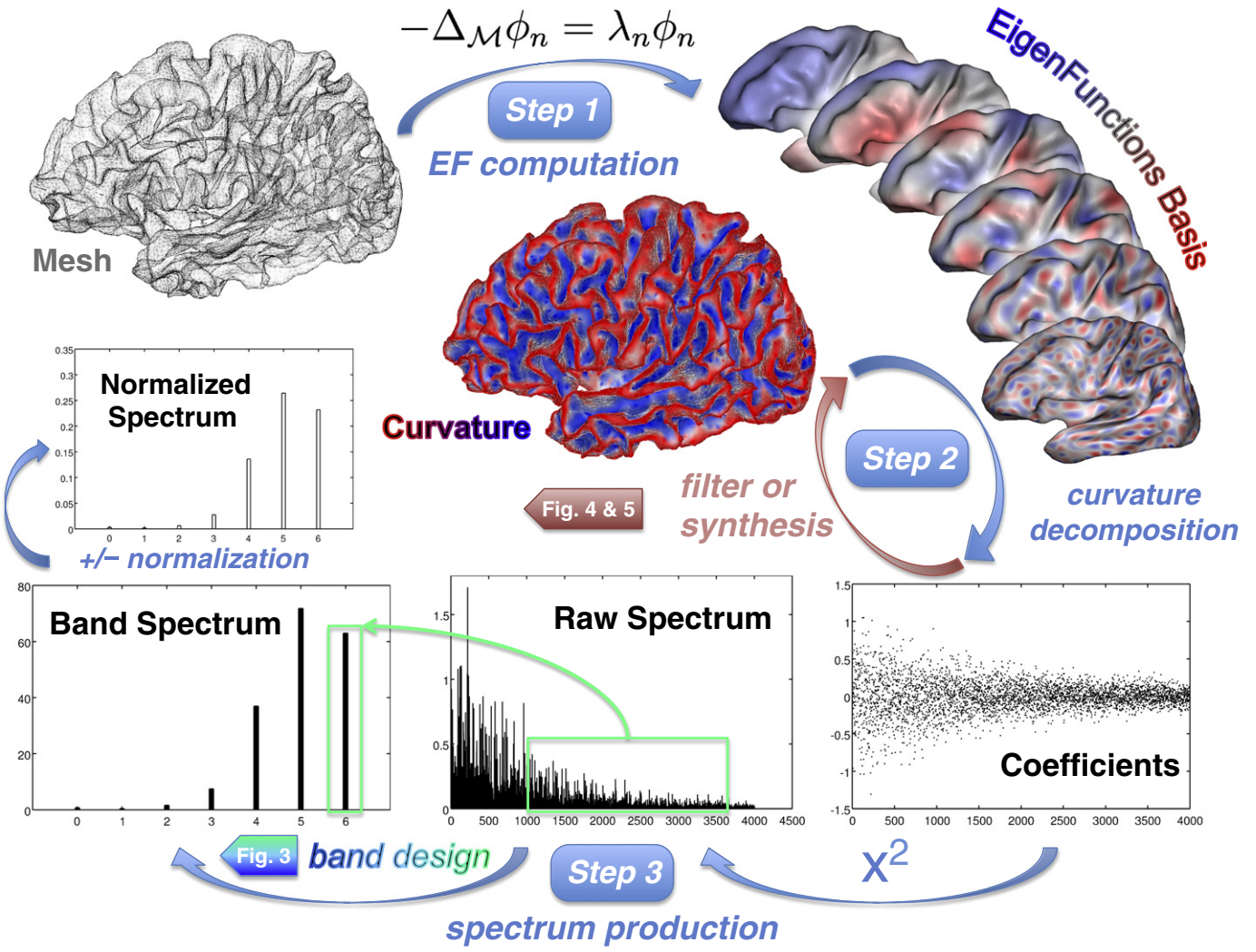

Fig. 2. Spangy process (Spectral analysis of gyrification). Step 1: The *computation of the eigenfunctions* (EF) of the Laplace–Beltrami operator of the cortical mesh provides the decomposition basis for spectral analysis. Step 2: The *decomposition of curvature* on the eigenfunctions basis gives a series of coefficients that are characteristic of the curvature in the spectral domain. This step is reversible, which allows spectral filtering of the curvature and thus, supports the spectral segmentation of cortical folding pattern explained in Figs. 4 and 5. Step 3: The *production of the band power spectrum* of curvature from the squared coefficients relies on the band design choices detailed in Fig. 3a.

$\lambda_1 \leq \ldots$the *eigenvalues* of $-\Delta_{\mathcal{M}}$ and $\phi_0, \phi_1, \ldots$ an associated orthonormal basis of eigenfunctions in $L^2(\mathcal{M})$ that satisfy:

$$-\Delta_{\mathcal{M}}\phi_i = \lambda_i\phi_i. \tag{1}$$

Given an eigenfunction ϕ_i, the nodal set of ϕ_i is defined as $\{x \in \mathcal{M}, \phi_i(x) = 0\}$. The connected components of the complement of the nodal set are called *nodal domains*. The Courant Nodal Domain Theorem ensures that if ϕ_i is not the first eigenfunction, the number of nodal domains is at least 2 and at most i. Moreover any function $u \in L^2(\mathcal{M})$ can be decomposed in the previous basis:

$$u = \sum_{i=0}^{+\infty} u_i\phi_i, \text{ with } u_i = \int_{\mathcal{M}} u\phi_i. \tag{2}$$

The Parseval's formula which will be useful for normalization states that:

$$\int_{\mathcal{M}} u^2 = \sum_{i=0}^{+\infty} u_i^2. \tag{3}$$

It is possible to compute eigenfunctions on a mesh $\hat{\mathcal{M}}$ that approximates $\mathcal{M}$ using a weak formulation of the eigenvalue problem and the finite elements method. If u and λ are solutions of $-\Delta_{\mathcal{M}}u = \lambda u$ then:

$$\int_{\mathcal{M}} g(\nabla u, \nabla v) = \lambda \int_{\mathcal{M}} uv, \forall v \in L^2(\mathcal{M}). \tag{4}$$

We use the finite elements framework to derive a matricial expression of this weak formulation. We consider the mesh $\hat{\mathcal{M}}$ composed of N vertices. For each vertex i of the mesh we have a function $w_i : \hat{\mathcal{M}} \to \mathbb{R}$ which is continuous, linear on each triangle of the mesh and satisfying the property $w_i(j) = \delta_{ij}$. Any function continuous and linear on each triangle can be decomposed on this basis $u = \sum_{i=1}^{N} u_i w_i$ where u_i are real coefficients. So Eq. (4) can be rewritten in the discrete setting, taking $v = w_j$ for all $j \in [1:N]$. And the discretized problem is then to find a vector $[U] = (u_i)_{i=[1:N]}$ and a scalar λ such that:

$$[\nabla][U] = \lambda[M][U], \tag{5}$$

with the stiffness and mass matrices given by :

$$[\nabla] = \left(\int_{\hat{\mathcal{M}}} \nabla w_i \cdot \nabla w_j\right)_{i=[1:N],\, j=[1:N]}, [M] = \left(\int_{\hat{\mathcal{M}}} w_i w_j\right)_{i=[1:N],\, j=[1:N]}.$$

More details on the computation of these two matrices are given in Desbrun et al. (1999). The eigenvalue problem (5) can be solved for example with the Lanczos method as in (Arnoldi Package) since the matrices involved are sparse and symmetric positive.

In practice, we computed several thousand eigenfunctions (5000) such that the spatial wavelength reaches a reasonable spatial resolution (see B).

Curvature decomposition (Step 2)

The mean curvature (C) can be decomposed in the eigenfunction basis through formula (2). We will denote $C_i := \int_{\mathcal{M}} C\phi_i$ the (Fourier) coefficients of the curvature in the eigenfunctions basis ϕ_i and call *raw spectrum* the sequence $RS_C(i) := C_i^2$. We define also a normalized spectrum of curvature:

$$NS_C(i) := \frac{C_i^2}{\int_{\mathcal{M}} C^2} \forall i \geq 0. \tag{6}$$

which satisfies:

$$\sum_{i=0}^{+\infty} \mathrm{NS}_C(i) = 1 \tag{7}$$

thanks to Parseval's formula (3).

We call *Total Folding Power* the quantity:

$$\mathrm{TFP}_C := \sum_{i=0}^{+\infty} C_i^2 = \int_{\mathcal{M}} C^2 \tag{8}$$

This dimensionless parameter is independent of homothetic brain size variation. Namely, if one has a scaling coefficient λ between $\mathcal{M}_1$ and $\mathcal{M}_2$ then $C_{\mathcal{M}_2} = \frac{1}{\lambda} C_{\mathcal{M}_1}$ and a small quantity of surface becomes $dS_2 = \lambda^2 dS_1$, and then:

$$\int_{\mathcal{M}_2} C_{\mathcal{M}_2} dS_2 = \int_{\mathcal{M}_1} C_{\mathcal{M}_1} dS_1 \tag{9}$$

Spectral frequency bands design (step 3)

In the following, we will call $F(i)$ and $\mathrm{WL}(i)$ the theoretical frequencies and the wavelengths associated to the ith eigenfunction λ_i (see A for further development on spatial frequencies):

$$F(i) = \frac{1}{\mathrm{WL}(i)} = \frac{\sqrt{\lambda_i}}{2\pi} \tag{10}$$

As a consistency check we compared these theoretical wavelengths with eigenfunction-derived quantities of the same dimension, which can be intuitively considered as empirical wavelengths and can be computed based on the number of nodal domains through the formula:

$$\mathrm{WL}_E(i) = \sqrt{\frac{\text{Area of } \mathcal{M}}{\text{Number of nodal domains of } \phi_i}} \tag{11}$$

The raw spectrum of curvature is a very complex type of data, challenging to analyze and even to visualize because of its several thousand points. Moreover, since the eigenfunctions are defined on a per-individual basis, there is no mathematically exact matching of eigenfunctions of the same i-order (Knossow et al., 2009; Lombaert et al., 2011). Hence, as a dimensional reduction and smoothing step, we merged levels of successive orders into superior grouping levels defined by a sequence of spatial frequency $F(i)$ marking interval limits. The sequence was chosen in order to fulfill a model of branching with doublings of spatial frequency. The spatial frequency associated with the first non-constant eigenfunction was considered as the subject's reference frequency $F(1)$. The following interval limits were the spatial frequencies $2^k F(1)$. This merging strategy allowed us to define a band power spectrum (than could be later normalized or not) defined as:

$$BS_C(0) = C_0^2 \tag{12}$$

$$BS_C(k) = \sum_{i=i_1^k}^{i_2^k} C_i^2 \text{ with} \tag{13}$$

$$i_1^k = \arg\min_i \left| F(i) - 2^{k-1} F(1) \right| \tag{14}$$

$$i_2^k = \arg\min_i \left| F(i) - 2^k F(1) \right| \tag{15}$$

As we computed around 5000 eigenfuntions, this merging strategy allowed us to define 7 bands, numbered from B0 to B6. See Fig. 3 for band design steps.

Spectral segmentation of cortical folding pattern

We define a CFP map as the binary map where sulci correspond to regions of negative curvature and gyri correspond to regions of positive curvature. Based on the properties of spectral decomposition, band-by-band spectral synthesis of curvature can be performed in a cumulative or non-cumulative way. Non-cumulative synthesis is equivalent to band-pass filtering, and can be used to show the specific contribution of each spectral band. Cumulative synthesis, is equivalent to low-pass filtering, and can be used to show the effect of the gradual addition of higher frequency components to the map. From these 2 types of synthesis, we derived 2 segmentations of CFP (see Figs. 4 and 5 for steps summary):

- First, a segmentation according to the locally *dominant* frequency band: we used non-cumulative synthesis to label each vertex with the number of the band that contributed the most to its curvature value. The result of this segmentation process is a texture denoted S_{dom}. See Fig. 4 for computation steps.
- Second, a segmentation according to the locally *determinant* frequency band: we used cumulative synthesis to label each vertex with the number of the band that determined whether it belongs to the sulcal or the gyral pattern. We assessed the differential contribution of each frequency band to the CFP by subtracting between the CFP maps of two consecutive levels of cumulative synthesis. The result of this second segmentation process is a texture denoted S_{det}. See Fig. 5 for computation steps.

Extensive formulations for these 2 types of segmentation are given in C. For the sake of clarity, they can be both visualized with a gyral pattern mask, hence restricting the image to the sulcal pattern. Due to their large preponderance in patterning (see Results), second segmentation is restricted to the last three frequency bands.

For each label, we computed the total surface area and the number of parcels, i.e. sets of connected vertices that have the same considered label. The segmentation according to the locally dominant band is rather noisy due to the use of a truncated spectrum (number of eigenfunctions < number of vertices), which produces very small parcels (mainly isolated vertices) related to non-computed bands (very high frequencies). We thus used an adaptive-threshold filter to remove these noisy parcels before computation (see B). Conversely, for the segmentation according to the locally determinant band, the number of parcel related to each label had been directly computed on the intermediary subtraction step.

a)

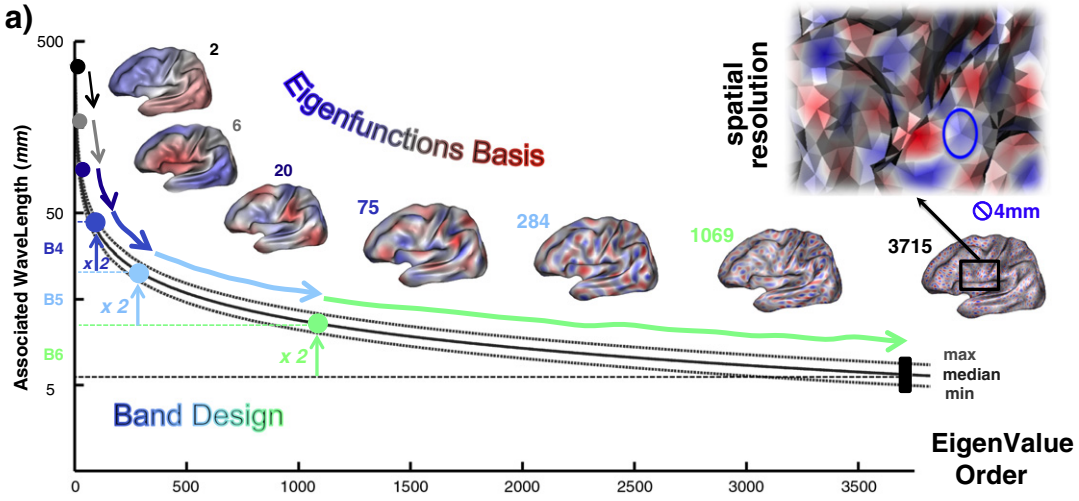

b)

	HV (cm^3)	HA (mm^2)	B1		B2		B3		B4		B5		B6		resolution	
			EV order	WL (mm)	EV order	WL (mm)	EV order	WL (mm)	EV order	WL (mm)	EV order	WL (mm)	EV order	WL (mm)	EV order	WL (mm)
mean	591	77327	2	447	6	212	21	110	78	56	296	28	1111	14	3832	7
SD	50	7623	0	24	0	12	1	6	4	3	12	2	41	1	142	0
min	445	57323	2	396	6	188	19	97	71	49	274	25	1036	12	3550	6
median	591	72780	2	445	6	211	21	110	78	56	295	28	1106	14	3823	7
max	759	97199	2	513	6	248	25	126	94	64	343	32	1267	16	4305	8

Fig. 3. Spectral banding. a) Spectral bands design: frequency intervals according to the doubling frequency hypothesis. The spatial resolution achieved is illustrated by the relative size of the nodal domains of the last eigenfunction of the basis and the edges of the cortical mesh (median size brain of the database). Log-linear plot. min, median, max: brain of minimum, median and maximum size of the database. b) Spectral sizing: brain size, bandwidth and spatial resolution (wavelength associated with the last eigenfunction of the basis) for the whole database. WL: wavelength, EV: eigenvalue/eigenvector.

Statistical analysis and allometric scaling

We preformed an ANOVA to assess the effect of age, sex, and hemispheric volume on hemispheric surface area and spectral parameters. The correlations between cortical surface parameters (hemispheric surface area, total folding power or spectral band power) and brain size (hemispheric volume) were tested assuming a power law:

$$Y = bX^a \tag{16}$$

We compared the scaling factor a in the equation with the value it should have when the scaling is isometric, i.e. presuming that 1 or 2 dimensional parameters scale with hemispheric volume as the 1/3 or 2/3 power respectively, and that folding power is constant. The estimation of a and b was performed using log-log linear fit.

All statistical analyses have been performed using SPSS version 16.0.

Results

Measuring properties: wavelength and spectral power

Wavelength reflects nodal domain size

The measuring properties of the proposed band power spectrum rely on the association of each LBO eigenfunction of the basis with a well-defined spatial frequency. Eigenfunctions of increasing order (i.e. smaller associated eigenvalue) show an increasingly scattered nodal domain pattern, consistent with the expected increase of their associated spatial frequency (Fig. 3a). The consistency between the empirical wavelength $\hat{D}$ estimated through the number of nodal domains $\hat{D}$ and the theoretical wavelength $\hat{D}$ derived from the eigenvalue $\hat{D}$ is confirmed by the strong linear correlation between the two values. For low orders, the empirical computation is not precise, due to its sensitivity to domain shape, coalescence and irregularity, but from the 10th order on, the relationship becomes almost exact (mean fit for ICBM database: $0.87x + 4.51$, $R = 1$), and after the 100th order, there no longer seems to be any difference ($0.97x + 0.56$, $R = 1$). In spite of a certain variability, the mean shape for the nodal domains of an eigenfunction looks like a spot scaled by its theoretical wave length (Fig. 3a). The wavelength not only depends on the order of the eigenfunction but also on the size of each individual brain. Being a one-dimensional parameter intrinsically derived from the grey/white surface, the theoretical wavelength is expected to scale as $HA^{1/2}$, which is almost exactly what we observe in the ICBM database: $1.74\ HA^{0.495}$, $R = 0.938$. This result validates the possibility of computing frequency band statistics in the ICBM database (Fig. 3b) which provide a standard for patterns sizing.

Spectral resolution achieves mesh resolution

The spatial resolution of our spectral analysis is limited intrinsically by the mesh resolution, and extrinsically by the number of eigenfunctions computed in the decomposition basis. The density of vertices in the surfaces that we used is not homogenous and changes locally depending on the surface geometry. The mean number of vertices in our surface reconstructions was 21418 ± 2268, and the mean triangle edge length was 2 mm $\pm$ 0.5 mm, i.e. a mean resolution of 3 mm^2. The mean wavelength of the last eigenfunction necessary to compute the proposed 7 bands is 7 mm, i.e. a mean resolution of 9 mm^2 (see Fig. 3a for illustration, Fig. 3b for values and Appendix B for computation). Hence, in our analyses the spatial resolution of the decomposition basis was slightly larger than that of the surface meshes. This allowed us to consider a minimal pattern element of around 3 contiguous vertices. This resolution is reasonable given that the patterns of interest in a cortical surface are hardly to be found below half a centimeter, and also to avoid variation due to

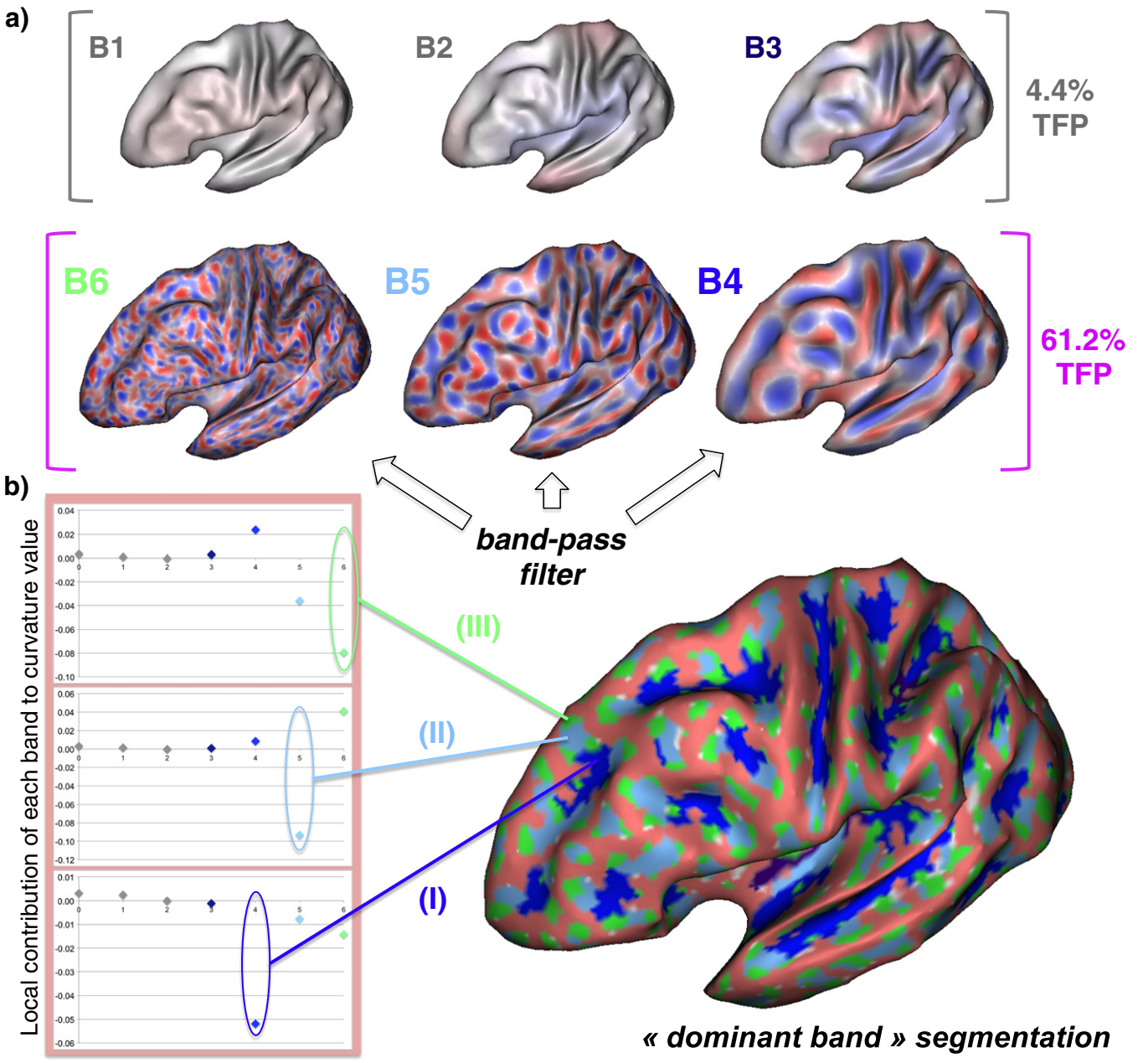

Fig. 4. Segmentation of cortical folding pattern (CFP) according to the locally 'dominant' band. a) Band-pass filtered curvature for the 6 spectral bands (1st and 2nd rows). The contribution of the bands to the total folding power (TFP) is only 4.4% for B1 + B2 + B3 but 61.2% for B4 + B5 + B6 which explains the differences in colour intensity. b) Plots show the decomposition of curvature at points (I) (II) and (III) obtained from the band-pass filtered series. On the right, each point of the surface is labeled with the band that contributes most to its curvature value, i.e. the "dominant" band. Segmentation is presented for median size brain on a smoothed anatomy with a gyral mask (salmon red).

inaccuracies in surface segmentation and reconstruction. To assess the robustness of our results with respect to the number of vertices of the meshes, we compared the spectrum computation before and after mesh refining (doubling of the number of vertices) , and we did not find any significant differences (data not shown).

Spectral power concentrates in the last 3 bands

By construction, the proposed band power spectrum gives a partition of the total folding power in intervals of doubling spatial frequencies (i.e. spectral bands). The band power spectrum normalized by the total folding power provide a spectral proportion, or in other terms, the relative weight of each spectral band. However, the decomposition basis necessary for the computation of 7 bands cannot account for the full total folding power since part of it is contained in the higher frequency levels that we do not compute. The normalized 7 bands spectra of all ICBM database subjects shows that on average, our analysis concerns around 2/3 of the total folding power (mean 65.8%, SD 1.45%). More precisely (Figs. 4a and 6):

- B0 (the constant band) accounted for 0.35% (SD 0.14%),
- B1, 2 and 3 (the first 3 oscillating bands) accounted for 4.39% (SD 0.79%),
- B4, 5 and 6 (the last 3 oscillating bands) accounted for 61.2% (SD 1.43%).

This shows the quantitative predominancy of the last 3 bands, which account for a large proportion of the total folding power and almost the totality of the analyzed folding power (92.8%).

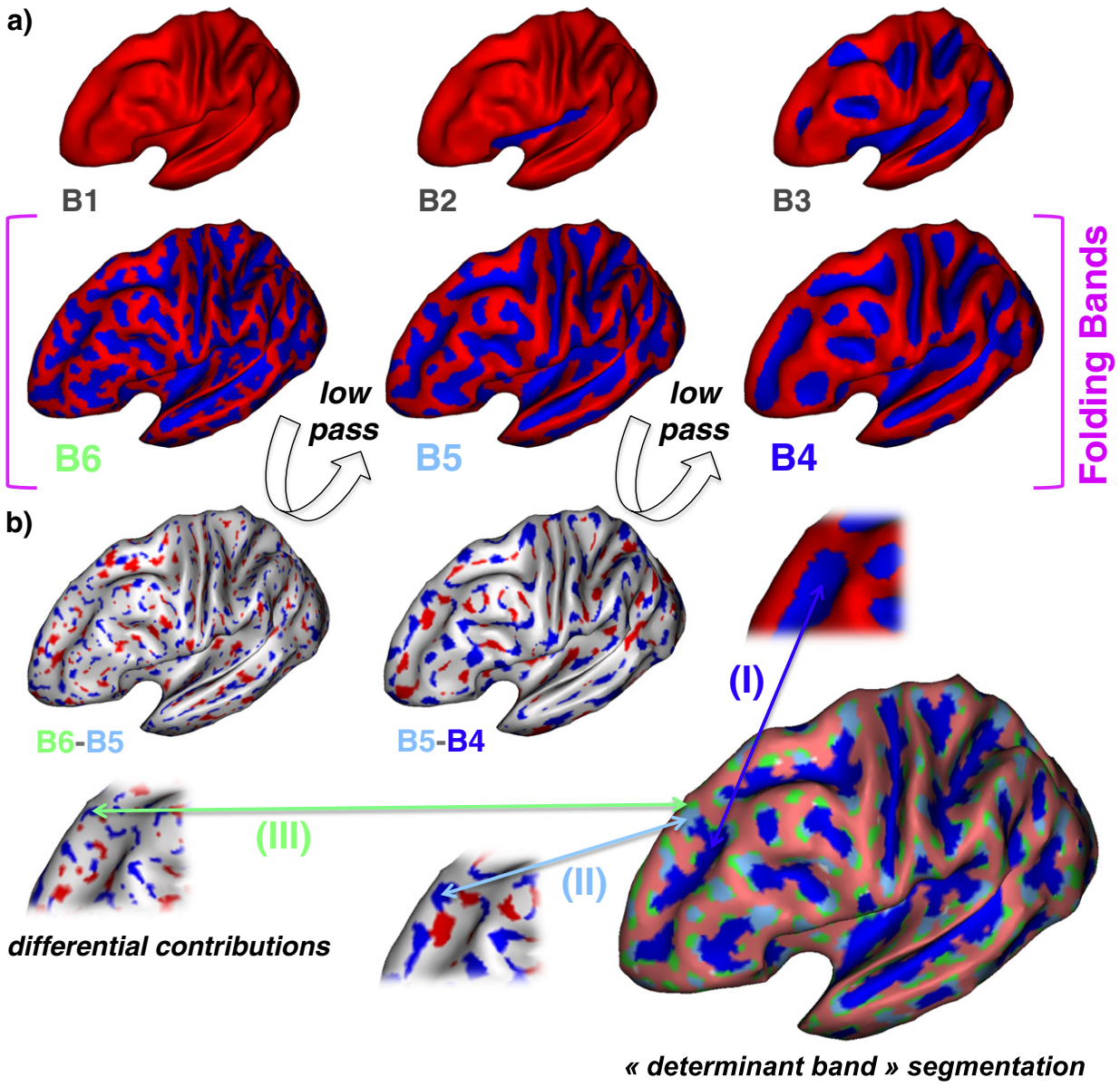

Fig. 5. Segmentation of cortical folding pattern (CFP) according to the locally 'determinant' band. a) Low-pass filtered CFP series for the 6 spectral bands (1st and 2nd rows). The folding Bands, i.e. B4, B5 and B6, account for folds-related patterns. b) The differential contribution of B6 and B5 (3rd row) is given by subtraction between two consecutive levels of filtering. Magnifications show the vicinity of points (I) (II) and (III). On the right, each point of the surface is labeled with the band that determines whether it belongs to the sulcal or the gyral pattern, i.e. the "determinant" band. Segmentation is presented for median size brain on a smoothed anatomy with a gyral mask (salmon red).

Describing properties: anatomical–spectral correlations

We now show the utilization of Spangy to categorize and quantify pattern elements back on the original cortical surface, on the basis of spatial frequency properties.

'Global shape bands' vs 'folding bands'

Low-pass and band-pass filtering provide a first insight into the link between spectrum and cortical folding through the sequential visualization of the contribution of each band to the curvature value (Fig. 4) and the CFP (Fig. 5). B0 does not account for any pattern since the 1st eigenfunction does not oscillate. B1 and B2 bands account for patterns that are not correlated with folding but rather with the global brain shape, like the slight concavity of the medial hemispheric side (B1) and the bottom of the sylvian fissure (B2), the global convexity of the lateral hemispheric side (B1), or the convexity of the polar regions (B2). B3 not only contributes mainly to the global brain shape with the transition between lateral and medial sides of the hemisphere or the sylvian banks, but also to initiate the fundi of several primary sulci, such as the posterior part of the superior temporal sulcus or the medial part of the intra parietal sulcus. As we have shown previously, whatever the qualitative contribution to the CFP of the first three non-constant bands may be, they are quantitatively very weak. Thus, patterns consistent with cortical folding appear with B4 (Figs. 4a, 5a) and most substantial contributions to the CFP are produced by B4, B5 and B6. *These 3 bands will be further referred as the 'folding bands'.*

Complementarity between dominant and determinant band segmentations of CFP

The 2 types (Figs. 4b and 5b) of spectral segmentation of CFP are presented in Fig. 7 on 5 brains of increasing size (restricted to sulcal

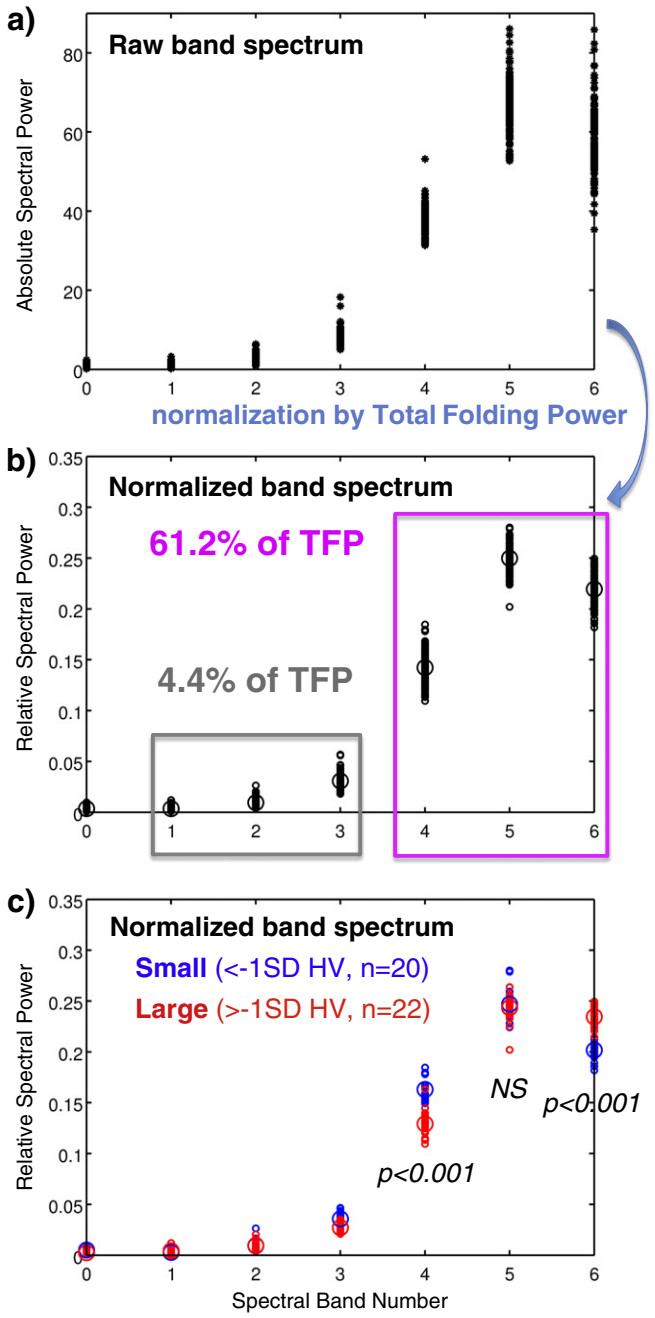

Fig. 6. Relative contribution of each band to the power spectrum of curvature. a) Raw band spectrum (whole dataset). b) Spectral proportions (whole dataset), obtained after normalization of the raw band spectrum by the total folding power (TFP). c) Effect of brain size i.e. hemispheric volume (HV). Differences of spectral proportions between small (HV below mean − 1SD) and large (HV over mean + 1SD) brains. Student *t* test. Large brains show a relative increase in high frequencies (B6) and a relative decrease of lower frequencies (B4). Large circle: mean value, NS: non-significant.

pattern): the segmentation according to determinant band in the 2nd column, and the segmentation according to dominant band in the 3rd column. They provide complementary information about the contribution of each folding band. The segmentation according to determinant band sums up the observations made on low-pass filter series and provides a clear image of the progressive ramification of the sulcal pattern produced by the addition of higher frequency bands. The segmentation according to dominant band shows a similar phenomenon but with significant differences in surface labeling which show that a vertex can be added to either sulcal or gyral pattern by one band, whereas its curvature value is mainly determined by a higher frequency band. These discrepancies between locally determinant frequency band and locally dominant frequency band are particularly visible around the polar regions. Besides, as previously explained, the segmentation according to dominant band is noisy and we applied a band-adapted minimum threshold for size before the quantification of surface area and number of sulcal parcels. This threshold had a very mild effect on the regions labeled by B4, B5 and B6, leading to a mean area reduction of respectively 6.9%, 1% and <0.1% (SD 1.5%, 0.2% <0.1%). Nonetheless, it was sufficient to rub out most of the irrelevantly small spots, particularly for B4 band, rejecting an average of respectively 118, 45 and 3 spots (SD 19, 11 and 2), with a mean spot area 2 times below the threshold. Finally, we found a strong linear correlation between B4, B5 and B6 spectral power and labeled surface area, respectively: $335x+3660$ ($R=0.783$), $396x-96.3$ ($R=0.917$), $403x+884$ ($R=0.961$), showing that the segmentation according to dominant band gives a faithful picture of the band power spectrum. The correlation was equally good between the normalized band power and the labeled surface area reported to hemispheric surface area.

Anatomical correlates of spectral segmentation of CFP

The sulcal pattern of the low-pass filtered CFP map at B4 level consists in a limited set (21 elements ± 3) of large smooth sulcal parcels with few ramifications (Fig. 7, 1st column). These spectrally defined folding fields embed the main primary folds of the literature (Fig. 8a, (Chi et al., 1977)) and are refined by B5 and B6 to produce a more irregular and branched CFP. According to the proposed spectral segmentations, the CFP can be divided into 1st, 2nd and 3rd order elements associated respectively with frequency bands B4, B5 and B6. These 3 orders are sufficient to describe the whole CFP even for dominant band segmentation which could have concealed up to 7 labels. Indeed, lower frequency band labeling is strictly restricted to B3 and only concerns a few deep sections of the superior temporal sulcus, intra parietal sulcus or insula, covering a very small percentage of the total sulcal area (<5%). The anatomical correlates of this 3-order segmentation are well illustrated by the analysis of the pericentral region in 3 reference brains of increasing size (Fig. 8b). The figure shows the straight course of the 1st order central element, the 2 or 3 loops corresponding to 2nd order elements and the small dimples associated with 3rd order elements, which are much more accentuated in the largest brain. The same anatomical correlations can be observed for gyral pattern and yet, for the whole CFP (Fig. 8c). Hence, we show that the distribution of 2nd and 3rd order elements of pattern is neither random nor homogeneously underlying the limits of lower order elements, but rather parsimoniously matches the gradual ramification of CFP from the previously defined 1st order folding fields.

Spectral composition of CFP as a function of brain size

Allometric scaling of surface area and folding power

We used the hemispheric volume (HV) as a brain size parameter. In our dataset, HV ranged from 445 cm^3 to 759 cm3, i.e., a 1.7-fold variation (Fig. 3b). The hemispheric surface area showed a positive allometric scaling: $HA=0.209HV^{0.961}$ ($R=0.950$, $p<0.001$, confidence interval [0.935, 0.987]), i.e. large brains had disproportionately more cortical surface than smaller brains. We found the same variation with brain size for the sulcal pattern area and the gyral pattern area, demonstrating the absence of allometric modification of sulcal versus gyral proportions: sulcal pattern area = $0.127HV^{0.951}$ ($R=0.953$, $p<0.001$, CI [0.926, 0.976]); gyral pattern area = $0.0828HV^{0.972}$ ($R=0.898$, $p<0.001$, CI [0.934, 1.012]). Total folding power also showed a positive allometric scaling, consistent with the fact that large brains are not simply scaled-up versions of smaller ones: total folding power = $8.16\times10^{-3}HV^{0.781}$ ($R=0.784$, $p<0.001$, CI [0.73, 0.832]).

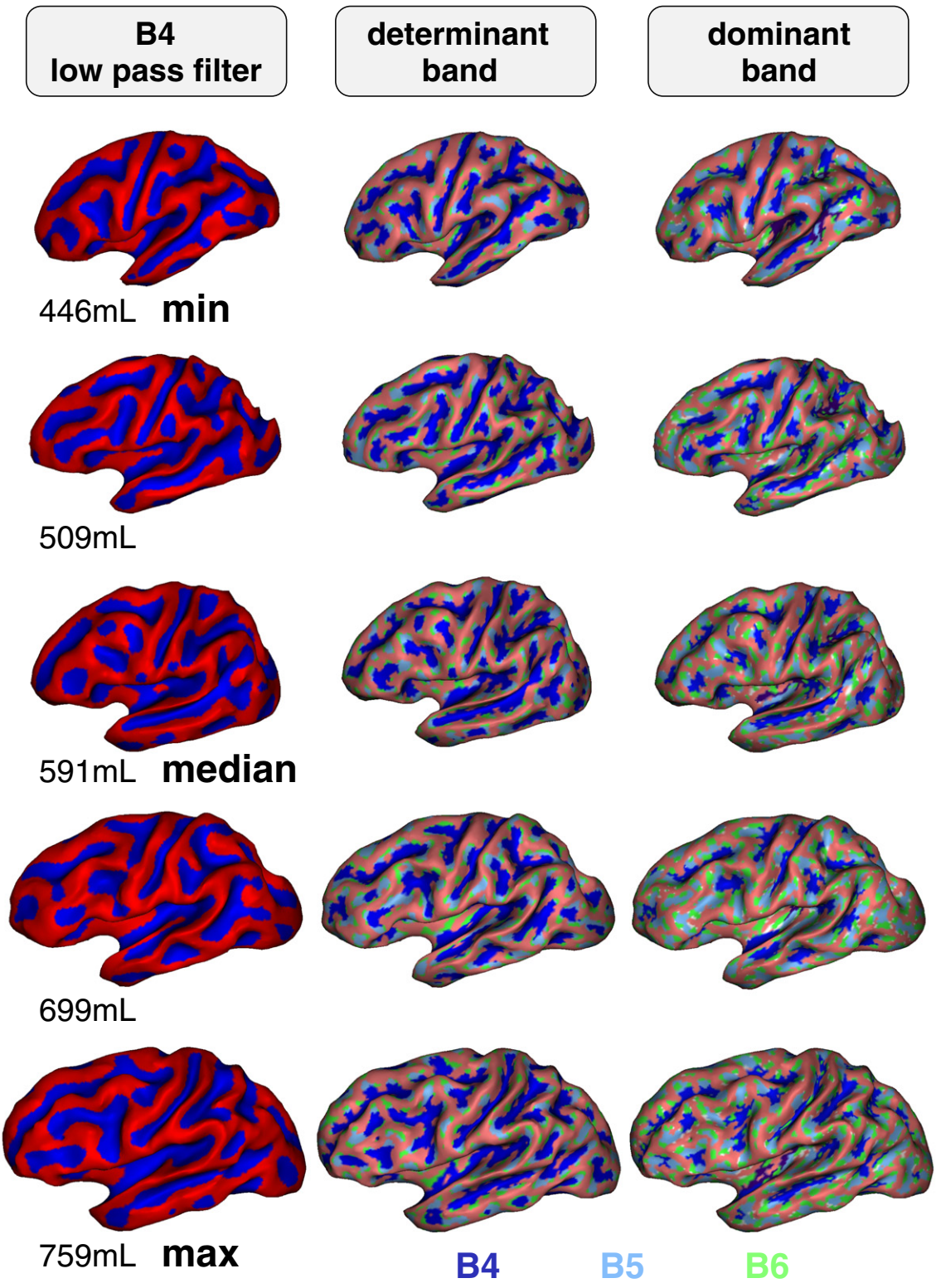

Fig. 7. Spectral segmentation of cortical folding pattern (CFP) in brains of increasing size. The 5 brains correspond to a sample of the dataset from smallest (min) to the largest (max), including the median and 2 intermediary size brains. Brains size is measured by hemispheric volume (HV). 1st column: B4 low-pass filtered CFP showing the constant number of primary folding fields. 2nd column: segmentation according to determinant band showing increase of B6 tagged ramifications with size. 3rd column: segmentation according to dominant band showing extension of B5 and B6 tagged surface. CFP segmentation is presented on a smoothed anatomy with a gyral mask (salmon red).

We used these allometric exponents as references for the scaling exponents found for subdivisions of the hemispheric surface (1st, 2nd and 3rd order elements of CFP) and total folding power (B4, B5 and B6).

Spectral allometry: different brain size means different spectral proportions

As they accounted for more than 90% of the analyzed folding power, we limited the following analysis to the folding bands. The largest proportion of the variance in spectral band power was related

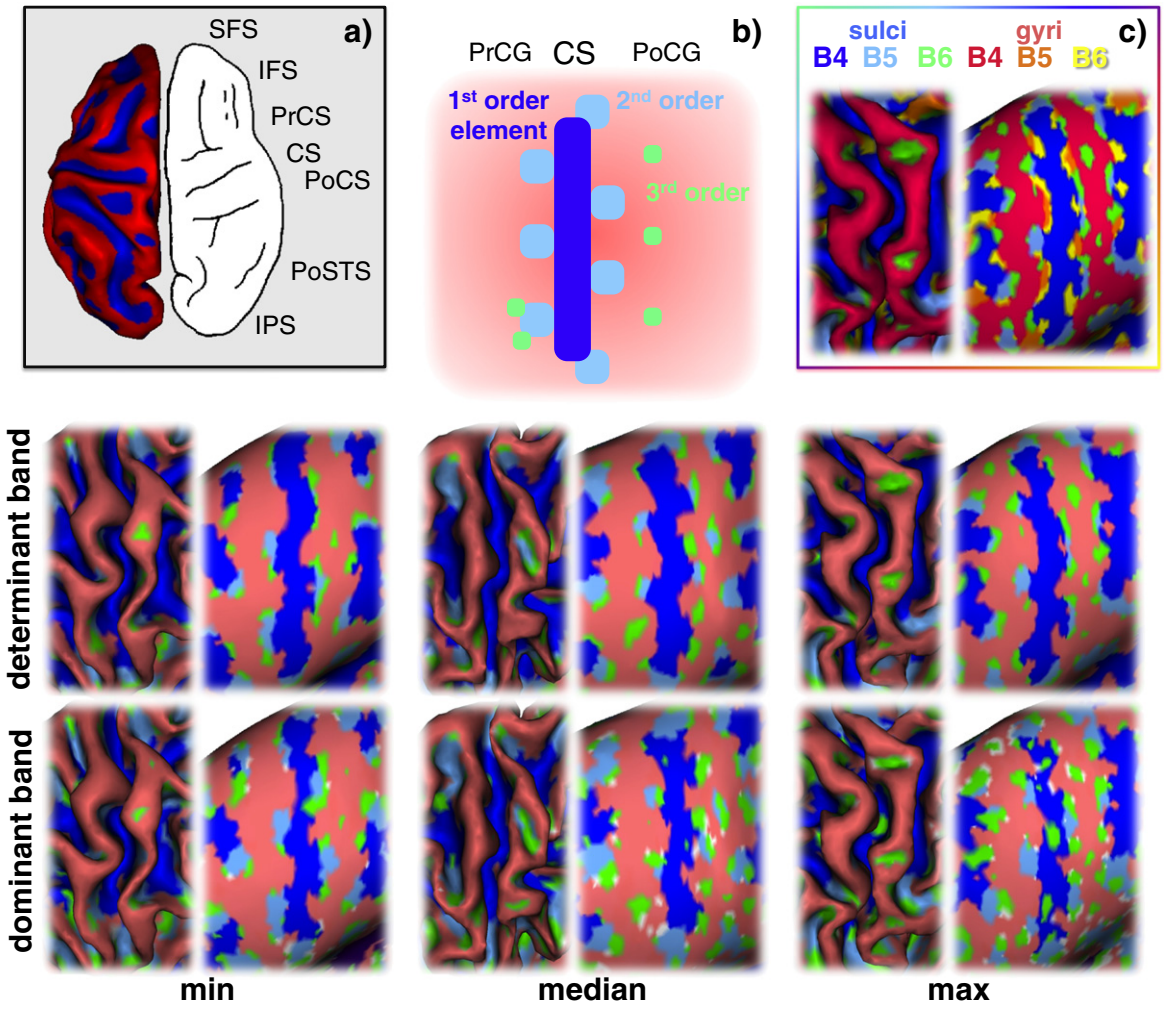

Fig. 8. Anatomical–spectral correlations. a) Primary folding fields correspond to B4 low-pass filtered CFP. Comparison between typical B4 low-pass filtered CFP and primary folds adapted from Chi et al. (1977). SFS: superior frontal sulcus, IFS: inferior frontal sulcus, PrCS: pre-central sulcus, CS: central sulcus, PoCS: post-central sulcus, PoSTS: posterior branch of the superior temporal sulcus, IPS: intra-parietal sulcus. b) Spectral segmentations of the central region: 1st, 2nd and 3rd order elements of CFP. Schematic interpretation of the segmentations is given in the 1st row (the number of 3rd order elements is arbitrary as it increases with brain size). 2nd row shows the segmentation according to determinant band. 3rd row shows the segmentation according to dominant band. For each brain, the segmentation is presented on the native (left) and totally smoothed (right) anatomy with a gyral mask (salmon red). min, median, max: brain of the database of minimum, median and maximum size. PrCG: pre-central gyrus, CS: central sulcus, PoCG: post-central gyrus. c) Spectral segmentation of the CFP in the central region without gyral masking. Spectral segmentation of sulcal and gyral pattern approximately mirror each other. Branching of the CFP is almost always associated with either a sulcal or a gyral higher order element. The segmentation according to determinant band is presented on the native (left) and smoothed (right) anatomy of the largest brain of the database.

to brain size variation ($R^2 = 61\%$ in a centered model) with no significant effect of age, sex, or handedness. Normalized band spectrum revealed a significant effect of brain size on spectral proportions (Fig. 6c). Large brains (standard score for HV > Mean + 1SD) showed a significantly larger proportion of B6 high spatial frequencies than small brains (standard score for HV < Mean − 1SD) and conversely, they showed a smaller proportion of B4 low spatial frequencies ($p < 0.001$ in both cases). The proportion of B5 medium spatial frequencies was not significantly different between the large and small brains. To further investigate the relationship between brain size and curvature band power spectrum, we compared the scaling of each spectral band power with the scaling of total folding power (Fig. 9a). We found no correlation between brain size and folding power for B4, an allometric exponent similar to that of total folding power for B5 (0.753 ± 0.052 versus 0.781 ± 0.051) and a higher allometric exponent of for B6 (1.213 ± 0.061 versus 0.781 ± 0.051). This shows that in large brains the larger proportion of B6 spatial frequencies compared with B4 and B5 is due to an increased contribution of these high frequencies to CFP rather than to a decrease of B4 ones. It also explains the stable proportion of B5 frequencies since total folding power is the normalization constant. In other terms, B4 contribution to the CFP is independent of brain size i.e. isometric scaling, B5 contribution follows the average increase of folding power with brain size i.e. positive allometric scaling, and B6 contribution increase faster than average i.e. the positive allometry is stronger for the higher spatial frequencies.

CFP complexity increases with brain size

How do the different behaviors of each folding band translate in terms of CFP? The computation of surface area and number of sulcal parcels for each label of the segmentation according to dominant band is presented in Fig. 9b and c. The variation of surface area with brain size for each order of CFP elements showed a specific behavior similar to that of frequency band power: increase of area with brain size is very slow for 1st order (B4), parallel to surface extension for 2nd order (B5) and faster than expected for 3rd order (B6). This result was robust and not sensitive to filter suppression of the noisy parcels. The number of parcels was independent of brain size for 1st and 2nd

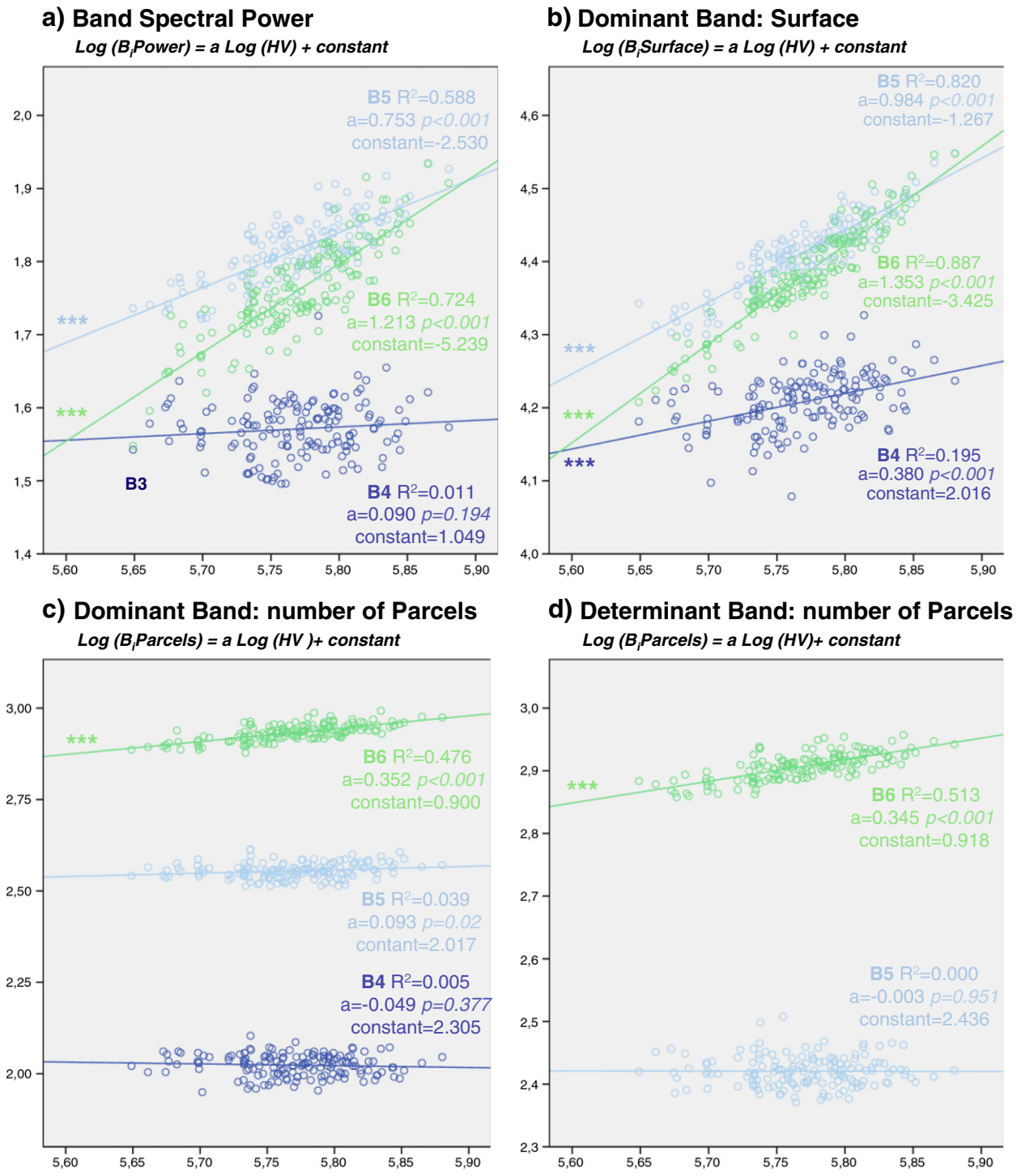

Fig. 9. Allometric scaling for cortical folding pattern (CFP) extension: larger brains are twistier because of an increased number of high spatial frequency elements. Data are shown in Log-Log plot, linearizing the power-law model $Y = bX^{a}$. *** show noteworthy correlation ($R^2 > 0.04$) and significant model fit ($p < 0.01$). a) Band spectral power scaling. Isometry for B4 (B4 power is independent of size), positive allometry for B5 (same scaling exponent as Total Folding Power = 0.76), accentuated positive allometry for B6 (scaling exponent = 1.21). b) Scaling of the surface of dominance for each band. The surface of dominance shows the same scaling as the band spectral power but with the scaling exponents of a 2 dimensional parameter. c) Scaling of the number of parcels of dominance for each band. The number of parcels is independent of brain size for B4 and B5 but increases for B6. d) Scaling of the number of parcels for each determinant band. Same scaling as the number of parcels of dominance. The number of parcels in B4 low-pass filtered CFP is 21 ± 3, also independent of brain size ($R^2 < 0.001$) (not shown due to figure scale).

order i.e. constant in spite of surface extension, while the number of parcels increased for 3rd order (Fig. 9c). This result was of course sensitive to filter suppression but we found the same behavior for each order with the segmentation according to determinant band that provides an even clearer image of the progressive ramification and do not require filtering (Fig. 9d). We found no significant differences between the analysis restricted to the sulcal pattern and that of the whole CFP. Hence, the proposed spectral segmentation allows the characterization and quantification of the increase in CFP complexity with brain size, demonstrating that it consists in a high frequency add-on

of folds and ramifications, as suspected by visual comparison of smaller and larger brains of the dataset (Figs. 7 and 8b).

Discussion and conclusion

The proposed Spectral Analysis of Gyrification (Spangy) methodology achieves a categorical and quantitative analysis of cortical folding pattern (CFP) both in the frequency domain through a band power spectrum and in the image domain with an anatomically relevant spectral segmentation. The computation is directly performed on native cortical meshes without the need for spherical parameterization or template normalization.

Sensitivity to data quality and preprocessing

The choice of the mean curvature of the grey-white interface as the best proxy of CFP could be questioned. Other continuous scalar functions defined on a cortex derived surface mesh could have been elected. Cortical thickness has been analyzed in a recent work (Cho et al., 2012), but is likely not a good CFP proxy. Actually, the mean curvature defines two gyral and sulcal patterns of almost equal areas on the grey-white interface, but not on external cortical surface (i.e. pial surface) where the CFP is very unbalanced. Future work with Spangy will try to use this external surface or even an intermediate surfaces such as that proposed in Van Essen et al. (2001). It would also be of interest to look for invariants between spectra computed on the same brains but with different surfaces or folding proxies (Gaussian curvature, sulcal depth, etc.). Besides the choice of the surface, the quality of data sets and preprocessing tools could affect the analysis, as in all sensitive morphometric tools. Indeed, if secondary mesh refinement (computational vertex density augmentation) does not seems to impact much on results, a primary higher mesh resolution could bring new spatial frequencies components out of the background noise. However the accuracy of brain segmentation methods is a major determinant of the correct divisions of sulci that could affect any morphometric result and thus should be tested through different softwares (BrainVisa, FreeSurfer, FSL for instance) or even software releases (Gronenschild et al., 2012). In particular we are currently checking to which extent our results on global CFP allometric scaling and local segmentation are reproducible with new datasets and new Morphologist Releases.

The model behind the frequency bands

The frequency-doubling model that we used to design frequency bands is a corner stone of the analytical properties of Spangy. This choice fits well with physical models of folding, and presents several convenient properties we did not observe with other models.

First, it provides an objective method to compare different subjects. Inter-subject matching of same-order eigenfunctions is a difficult problem, which complicates full ordinal comparisons between extended raw spectra (Knossow et al., 2009; Lombaert et al., 2011). Nonetheless, the proposed large frequency bands are equivalent to a large scale smoothing in the frequency space resulting in inter-subject relative frequency matching between bands of the same order. These bands are intervals of identical relative frequencies, meaning that they correspond to the same ratio of the fundamental frequency of each brain (i.e. the frequency given by the first non-null eigenvalue) even if they are composed by frequencies of different absolute values. This fundamental wavelength, which is empirically proportional to $HA^{1/2}$, can be seen as the geodesic length of the hemisphere (Lefèvre et al., 2012). In simpler terms, Spangy depicts CFP with a scale of brushes adapted to object size: larger touches are required for larger brains.

Second, it segregates the “folding bands” that clearly contribute to CFP from those that seem to account for global shape. This property could not be anticipated and we still have no model explaining the apparition of sulcal patterns with B4 ($2^3F(1)$ to $2^4F(1)$ spatial frequency range). Since this range is quantitatively large and the density of eigenfunction still rather low in this part of the spectrum, there is probably no exact frequency threshold above which CFP arises. This uncertainty concerning exact delineation of spectral folding frequency domain pleads for future implementation of intelligent models such as machine learning algorithms for CFP fundamental frequency assessment or for frequency clustering, with or without anatomically labeled learning data base. Nonetheless, the present strategy designs a convincing first folding band from which frequency doubling models make sense. Besides, our primary interest in CFP analysis with higher bands should not overshadow the clear association of low frequency bands with curvature variations related to global shape. Recent works suggest that the information gathered into these low frequencies may be relevant, at least for global shape classification (Niethammer et al., 2007; Lai et al., 2009), although their power is quantitatively small compared with that of the folding bands.

Third, it leads to a realistic segmentation of pattern ramifications. This property may directly result from the branching model that is behind the frequency sequence. Our results with spectral segmentation of CFP clearly show that this hypothesis is consistent with anatomical data and conversely support the validity of models predicting a frequency doubling with folding expansion. Interestingly, the bandwidth of the folding bands broadly accommodates the variation of dominant wavelength of same order elements of pattern between different regions of the brain. This appears clearly on the ‘determinant band’ segmentation (Fig. 5), where the first order patterns seem to be tighter in polar regions and wider in central ones.

From the frequency domain to the image space

Categorization

The segmentation proposed is free from anatomical or developmental *a priori*. Labeling is based only on spatial frequency characteristics of local curvature variations, or more precisely on how these local variations integrate into the whole pattern, since spectral analysis is not a local analysis. Our results on the central region show that we can distinguish two types of gradual contribution of the folding bands: firstly the termination of elongated elements of pattern, secondly the ramification of pattern both from an existing element and *de novo*. Termination labeling is of little anatomical meaning and rather due to strong impact of depth on surface based wavelength (see below). Conversely, ramification labeling is an interesting achievement. Indeed, starting from spectrally defined primary folding fields, Spangy segmentation categorizes 2nd and 3rd order of ramification or complexification of CFP (Fig. 8a, subsection "Anatomical correlates of spectral segmentaion of CFP") in a way that only developmental chronological follow-up had authorized up to now (Chi et al., 1977). To our knowledge, no other strictly morphological analysis has achieved this type of result so far.

Recent closely related mathematical tools such as fractal modeling (Yotter et al., 2011) allow estimation at global, regional and local scales, of a fractal dimension for the cortical surface thanks to spherical harmonics, but the authors have not applied their methodology to the segmentation or even the description of normal CFP. More intuitively, Laplacian smoothing has been presented as a possible tool for categorization of sulcal pattern elements since supposed tertiary folds seem to disappear earlier in the process than secondary, and so on (Cachia et al., 2003). However, it is a continuous process depending on a scale parameter t whose relevant values vary from a fold to another and across subjects. It is also interesting to note that this process is not mathematically equivalent to filtering even if smoothing a map u till time t can be expressed from eigenvectors and eigenfunctions of Laplace–Beltrami Operator (same notations as in 2.2.1):

$$S_t(u) = \sum_{i=0}^{+\infty} u_i e^{-\lambda_i t} \phi_i \tag{17}$$

which is different from a truncated expression of Eq. (2):

$$T_N(u) = \sum_{i=0}^{N} u_i \phi_i \tag{18}$$

In many regions more intricate than the central region, local categorization of CFP elements is probably unattainable directly in the image space. The proposed spectral analysis integrates the whole pattern information in the frequency space for band power spectrum computation, but returns part of it locally in the image space with the segmentation according to the locally dominant frequency band. Hence, we are able to propose a spectral based segmentation even in complex regions such as prefrontal cortex for example (see Fig. 7). Regional implementation of our spectral strategy on a patch of mesh corresponding to an anatomical (e.g. frontal lobe) or a functional area (e.g. Broca) would be of interest. Nonetheless performing global or local inter-subject analysis of the segmentations is not a trivial objective, which relies on relevant parameterization or registration of the surfaces and computation of statistical parametric maps. Furthermore, full demonstration of concordance between spectral and developmental labeling of elements of CFP goes far beyond the scope of the present work and will certainly need further investigation, for instance on longitudinal data of developing brains.

Quantification

Spangy provides two types of quantitative information. First, the wavelength intervals associated with B4, B5 and B6 give a size for 1st, 2nd and 3rd order elements of CFP that can be seen as a surface-based or geodesic wavelength. Such a surface-based measure depends both on the local depth and the local width of the associated fold. Very few object-based morphometric data are available for cortical folds. The BrainVISA morphometric toolbox allows depth assessment for well-validated sulci models (Cykowski et al., 2008) but provides no ramification-based segmentation. Nevertheless, the magnitude order for central sulcus is consistent with B4 associated wavelength range (Mangin et al., 2004). Object-based definition and computation of other size parameters such as volume-based (Euclidian) or surface-based (Riemannian) wavelengths would be of great interest to compare with the measures provided by Spangy (Lefèvre et al., 2012). Indeed, accurate CFP morphometry could open the field of a new quantitative characterization of folding during development, aging or in congenital malformations such as lissencephaly (too few, too large folds) of polymicrogyria (too many, too tight folds) (Richman et al., 1975). Yet sizing of CFP elements is not enough for folding characterization, which requires assessing the global composition of CFP for each category. This composition is the second quantitative information provided by Spangy. Band power is probably the best assessment of each spatial frequency interval contribution to the CFP since spectral segmentation goes with certain loss of information: locally, an element of pattern can only be related to one band even if several folding orders are intricate Additionally, the proposed segmentations allow a count of categorized fold elements and ramifications back in the anatomical space. Ultimately, forthcoming research may provide normative chart of Spangy-derived parameters useful to understand abnormal brain development or aging and perhaps design new diagnostic criteria.

Beyond gyrification indices, a new measure of gyrification pattern complexity

In this work we propose a first application of the new approach provided by Spangy to answer the question of the relationship between brain size polymorphism and CFP complexity variation. The allometric relationship between brain size (hemispheric volume) and hemispheric surface area has been already reported (Toro et al., 2008). Some results even suggest that this allometry is not spatially homogeneous and that local gyrification indices increase more in some brain regions, prefrontal area for instance, than in others (Toro et al., 2008; Schaer et al., 2008). These indices inform us on the amount of buried cortical surface but are not able to distinguish between profuse shallow folds and rare deep ones. Hemispheric total folding power gives roughly the same information than hemispheric gyrification index: both are highly correlated ($R = 0.8$) but equally blind to shape and gyrification pattern. The band power spectrum provided by Spangy precisely unwraps this black box: the allometric increase of total folding power does not divide up equally between bands. Spangy reveals 3 orders of pattern elements of increasing spatial frequency bandwidth, which vary differentially with brain size. This phenomenon is well observed in our results on ICBM data set:

- The contribution to CFP of B4 low spatial frequencies is constant in terms of both spectral power and number of pattern elements.
- The contribution of B5 medium spatial frequencies increases with the same allometric exponent than total folding power but with a number of pattern elements still constant.
- The contribution of B6 high spatial frequencies shows both a much higher allometric exponent and an increased number of pattern elements.

Eventually, the increase of gyrification complexity can be seen as the allometric scaling of gyrification pattern, i.e. the extension of CFP both by ramification and by addition of disconnected new elements. To our knowledge, this is the first objective and quantitative demonstration of this phenomenon suspected by radiological observations. Larger brains are definitely twistier because of increased number of barbells, dimples and kinks of high spatial frequencies that accommodate the allometric increase of cortical surface to be buried.

Acknowledgments

We would like to thank Louis Collins and Alan Evans for having provided ICBM database. Jean François Mangin is funded by the Agence Nationale de la Recherche (ANR-09-BLAN-0038-01, "Brainmorph").

Appendix A. Definition of spatial frequencies

In one dimension, the eigenvalue problem (1) becomes

$$u''(x) = -\lambda u(x) \quad \forall x \in [0, L] \tag{A.1}$$

and the solutions are obtained through the sine and cosine functions depending on boundary conditions (Dirichlet or Neumann for instance). An eigenfunction can be expressed on the form $\cos\left(\frac{\pi n x}{L}\right)$ or $\sin\left(\frac{\pi n x}{L}\right)$ with n an integer that gives the number of oscillations of the eigenfunction and the corresponding eigenvalue is $\lambda_n = \left(\frac{\pi n}{L}\right)^2$. The frequency is classically defined as the inverse of the period or wavelength $\frac{2\pi}{\pi n/L}$ and therefore equals $\frac{\sqrt{\lambda_n}}{2\pi}$. In two dimensions we can have explicit formula in the case of a rectangular domain of size L and l and the eigenfunctions can be expressed in a decoupled way, for instance for Neumann boundary conditions:

$$\cos\left(\frac{\pi m x}{L}\right)\cos\left(\frac{\pi n y}{l}\right) \forall (x, y) \in [0, L] \times [0, l] \tag{A.2}$$

and the corresponding eigenvalue is $\lambda_n = \left(\frac{\pi m}{L}\right)^2 + \left(\frac{\pi n}{l}\right)^2$. Even if the concept of spatial frequency is ambiguous in 2D and depends on the oscillations along each direction x and y, we will consider that $\sqrt{\lambda_n}$ has the dimension of a spatial frequency.

Appendix B. Computation of resolution and thresholds

For a given spatial resolution of a mesh, let d be the average edge distance between two contiguous vertices. Then, the average sign inversion spot (an isolated point of different sign than its neighbors) is around $\pi(d/2)^2$ mm^2 large (small disc of d mm diameter). For a given eigenfunction basis spatial resolution, let WL be the wavelength associated with last eigenfunction of the basis. Then, it is associated with an average size spot of $\pi(WL/4)^2$ area (small disc of $WL/2$ mm diameter).

For the adaptative thresholding in 3, we have made a similar reasoning: a noisy parcel in band k is roughly approximated by a circular shape of radius R_k. So we have the relation for the characteristic size :

$$2R_k < \frac{1}{2}\frac{WL(1)}{2^k} \tag{B.1}$$

which implies that the area of the parcels satisfies:

$$A_k < \frac{\pi^2}{16}\left(\frac{WL(1)}{2^k}\right)^2 \tag{B.2}$$

The adaptative threshold for each spectral band k is therefore given by the right term in the previous equation.

Appendix C. Extensive formulations of the spectral segmentations

We give here the formula for the segmentation according to the locally dominant frequency band:

$$S_{\mathrm{dom}}(p) = \arg\max_{k>0}\left(\mathrm{sign}(C(p))\sum_{i=i_1^k}^{i_2^k} C_i\phi_i(p)\right)\forall p\in\mathcal{M} \tag{C.1}$$

The sign of the curvature indicates whether we are in a gyrus or a sulcus.

For the segmentation according to the locally determinant frequency band, we start by computing the differential contribution of each frequency band to the CFP by subtraction between the CFP maps of two consecutive levels of cumulative synthesis:

$$\forall p\in\mathcal{M}\quad SM_k(p) = a-b \text{ where} \tag{C.2}$$

$$a = 1 \text{ if } \sum_{i=1}^{i_2^k} C_i\phi_i(p) > 0 \text{ else } a = 0 \tag{C.3}$$

$$b = 1 \text{ if } \sum_{i=1}^{i_2^{k-1}} C_i\phi_i(p) > 0 \text{ else } b = 0 \tag{C.4}$$

Then, we follow the procedure explained graphically in Fig. 5: We start from SM_k for $k=6$ (third row, first column) which counts 3 labels -1 (blue), 0 (gray) or 1 (red). A vertex with label l will be assigned another label $3\,l$. Then we consider SM_k for $k=5$ (third row, second column) and to each vertex with label l not previously re-labeled we assign the label $2\,l$. The last step is achieved for $k=4$ where all vertices not re-labeled previously will keep their label l. Finally, the resulting segmentation S_{det} is represented with a gyral mask (last row) and counts 3 labels: -3 (green), -2 (cyan) and -1 (dark blue). Formally we have the formula:

$$S_{\mathrm{det}}(p) = k\mathrm{SM}_k(p)1_{[|-3,-1|]}(k)$$

References

Armstrong, E., Schleicher, A., Omran, H., Curtis, M., Zilles, K., 1995. The ontogeny of human gyrification. Cereb. Cortex 5, 56.

Arnoldi Package, http://www.caam.rice.edu/software/ARPACK/.

Berger, M., 2003. A Panoramic View of Riemannian Geometry. Springer Verlag.

BrainVisa Software, http://www.brainvisa.info/.

Cachia, A., Mangin, J., Riviere, D., Kherif, F., Boddaert, N., Andrade, A., Papadopoulos-Orfanos, D., Poline, J., Bloch, I., Zilbovicius, M., et al., 2003. A primal sketch of the cortex mean curvature: a morphogenesis based approach to study the variability of the folding patterns. IEEE Trans. Med. Imaging 22, 754–765.

Cachia, A., Paillère-Martinot, M., Galinowski, A., Januel, D., de Beaurepaire, R., Bellivier, F., Artiges, E., Andoh, J., Bartrés-Faz, D., Duchesnay, E., 2008. Cortical folding abnormalities in schizophrenia patients with resistant auditory hallucinations. NeuroImage 39, 927–935.

Chi, J., Dooling, E., Gilles, F., 1977. Gyral development of the human brain. Ann. Neurol. 1, 86–93.

Cho, Y., Seong, J., Jeong, Y., Shin, S., 2012. Individual subject classification for Alzheimer's disease based on incremental learning using a spatial frequency representation of cortical thickness data. NeuroImage 59, 2217–2230.

Chung, M., Hartley, R., Dalton, K., Davidson, R., 2008. Encoding cortical surface by spherical harmonics. Stat. Sin. 18, 1269–1291.

Crampin, E., Gaffney, E., Maini, P., 1999. Reaction and diffusion on growing domains: scenarios for robust pattern formation. Bull. Math. Biol. 61, 1093–1120.

Cykowski, M., Coulon, O., Kochunov, P., Amunts, K., Lancaster, J., Laird, A., Glahn, D., Fox, P., 2008. The central sulcus: an observer-independent characterization of sulcal landmarks and depth asymmetry. Cereb. Cortex 18, 1999.

Dale, A., Fischl, B., Sereno, M., 1999. Cortical surface-based analysis* 1: I. Segmentation and surface reconstruction. NeuroImage 9, 179–194.

Desbrun, M., Meyer, M., Schröder, P., Barr, A.H., 1999. Implicit fairing of irregular meshes using diffusion and curvature flow. Proceedings of the 26th annual conference on Computer graphics and interactive techniques, pp. 317–324.

Fischl, B., Rajendran, N., Busa, E., Augustinack, J., Hinds, O., Yeo, B., Mohlberg, H., Amunts, K., Zilles, K., 2007. Cortical folding patterns and predicting cytoarchitecture. Cereb. Cortex 18, 1973–1980.

Gronenschild, E., Habets, P., Jacobs, H., Mengelers, R., Rozendaal, N., van Os, J., Marcelis, M., 2012. The effects of freesurfer version, workstation type, and Macintosh operating system version on anatomical volume and cortical thickness measurements. PLoS One 7, e38234.

Gu, X., Wang, Y., Chan, T., Thompson, P., Yau, S., 2004. Genus zero surface conformal mapping and its application to brain surface mapping. IEEE Trans. Med. Imaging 23, 949–958.

Hübsch, T., Tittgemeyer, M., 2008. Multi-scale analysis of brain surface data. Mathematical Modeling of Biological Systems, Volume II, pp. 255–263.

Im, K., Lee, J., Lyttelton, O., Kim, S., Evans, A., Kim, S., 2008. Brain size and cortical structure in the adult human brain. Cereb. Cortex 18, 2181.

Knossow, D., Sharma, A., Mateus, D., Horaud, R., 2009. Inexact matching of large and sparse graphs using Laplacian eigenvectors. Graph-Based Representations in Pattern Recognition, pp. 144–153.

Kruggel, F., 2008. Robust parametrization of brain surface meshes. Med. Image Anal. 12, 291–299.

Lai, R., Shi, Y., Dinov, I., Chan, T., Toga, A., 2009. Laplace–Beltrami nodal counts: a new signature for 3d shape analysis. IEEE International Symposium on Biomedical Imaging: From Nano to Macro, ISBI'09, pp. 694–697.

Lefèvre, J., Germanaud, D., Fischer, C., Toro, R., Rivière, D., Coulon, O., 2012. Fast surface-based measurements using first eigenfunction of the Laplace–Beltrami operator: interest for sulcal description. IEEE International Symposium on Biomedical Imaging: From Nano to Macro, ISBI'12.

Lévy, B., 2006. Laplace–Beltrami eigenfunctions towards an algorithm that understands geometry. Shape Modeling and Applications, 2006. SMI 2006. IEEE International Conference on, IEEE, pp. 13–20.

Lombaert, H., Grady, L., Polimeni, J., Cheriet, F., 2011. Fast brain matching with spectral correspondence. Information Processing in Medical Imaging. Springer, pp. 660–673.

Luders, E., Narr, K., Thompson, P., Rex, D., Jancke, L., Steinmetz, H., Toga, A., 2004. Gender differences in cortical complexity. Nat. Neurosci. 7, 799–800.

Mangin, J., Riviere, D., Cachia, A., Duchesnay, E., Cointepas, Y., Papadopoulos-Orfanos, D., Collins, D., Evans, A., Régis, J., 2004. Object-based morphometry of the cerebral cortex. IEEE Trans. Med. Imaging 23, 968–982.

Mazziotta, J., Toga, A., Evans, A., Fox, P., Lancaster, J., 1995. A probabilistic atlas of the human brain: theory and rationale for its development: the International Consortium for Brain Mapping (ICBM). NeuroImage 2, 89–101.

Milner, R., 1990. The Encyclopedia of Evolution: Humanity's Search for Its Origins. Holt, New York.

Mora, T., Boudaoud, A., 2006. Buckling of swelling gels. Eur. Phys. J. E Soft Matter 20, 119–124.

Niethammer, M., Reuter, M., Wolter, F.E., Bouix, S., Peinecke, N., Koo, M.S., Shenton, M.E., 2007. Global medical shape analysis using the Laplace–Beltrami spectrum. Proceedings of MICCAI, pp. 850–857.

Paus, T., Otaky, N., Caramanos, Z., MacDonald, D., Zijdenbos, A., D'Avirro, D., Gutmans, D., Holmes, C., Tomaiuolo, F., Evans, A., 1996. In vivo morphometry of the intrasulcal gray matter in the human cingulate, paracingulate, and superior-rostra1 sulci: hemispheric asymmetries, gender differences and probability maps. J. Comp. Neurol. 376, 664–673.

Prothero, J., Sundsten, J., 1984. Folding of the cerebral cortex in mammals. Brain Behav. Evol. 24, 152–167.

Régis, J., Mangin, J., Ochiai, T., Frouin, V., Riviére, D., Cachia, A., Tamura, M., Samson, Y., 2005. "Sulcal root" generic model: a hypothesis to overcome the variability of the human cortex folding patterns. Neurol. Med. Chir. 45, 1–17.

Reuter, M., Wolter, F., Peinecke, N., 2006. Laplace–Beltrami spectra as [] shape-DNA of surfaces and solids. Comput. Aided Des. 38, 342–366.

Richman, D., Stewart, R., Hutchinson, J., Caviness Jr., V., 1975. Mechanical model of brain convolutional development. Science 189, 18–21.

Schaer, M., Cuadra, M., Tamarit, L., Lazeyras, F., Eliez, S., Thiran, J., 2008. A surface-based approach to quantify local cortical gyrification. IEEE Trans. Med. Imaging 27, 161–170.

Seo, S., Chung, M., 2011. Laplace–Beltrami eigenfunction expansion of cortical manifolds. IEEE International Symposium on Biomedical Imaging: From Nano to Macro, ISBI'11.

Striegel, D., Hurdal, M., 2009. Chemically based mathematical model for development of cerebral cortical folding patterns. PLoS Comput. Biol. 5.

Thompson, P., Schwartz, C., Lin, R., Khan, A., Toga, A., 1996. Three-dimensional statistical analysis of sulcal variability in the human brain. J. Neurosci. 16, 4261.

Toro, R., Perron, M., Pike, B., Richer, L., Veillette, S., Pausova, Z., Paus, T., 2008. Brain size and folding of the human cerebral cortex. Cereb. Cortex 18, 2352.

Van Essen, D., Drury, H., Dickson, J., Harwell, J., Hanlon, D., Anderson, C., 2001. An integrated software system for surface-based analyses of cerebral cortex. J. Am. Med. Inform. Assoc. 8, 443–459.

Watkins, K., Paus, T., Lerch, J., Zijdenbos, A., Collins, D., Neelin, P., Taylor, J., Worsley, K., Evans, A., 2001. Structural asymmetries in the human brain: a voxel-based statistical analysis of 142 MRI scans. Cereb. Cortex 11, 868.

White, L., Andrews, T., Hulette, C., Richards, A., Groelle, M., Paydarfar, J., Purves, D., 1997. Structure of the human sensorimotor system. I: morphology and cytoarchitecture of the central sulcus. Cereb. Cortex 7, 18.

Whitwell, J., Crum, W., Watt, H., Fox, N., 2001. Normalization of cerebral volumes by use of intracranial volume: implications for longitudinal quantitative MR imaging. Am. J. Neuroradiol. 22, 1483.

Yotter, R., Nenadic, I., Ziegler, G., Thompson, P., Gaser, C., 2011. Local cortical surface complexity maps from spherical harmonic reconstructions. NeuroImage 56 (3), 961–973.

Yousry, T., Schmid, U., Alkadhi, H., Schmidt, D., Peraud, A., Buettner, A., Winkler, P., 1997. Localization of the motor hand area to a knob on the precentral gyrus. A new landmark. Brain 120, 141–157.

Zilles, K., Armstrong, E., Schleicher, A., Kretschmann, H., 1988. The human pattern of gyrification in the cerebral cortex. Anat. Embryol. 179, 173–179.